

Physics of the 21cm line probe

- i. Historic overview
- ii. Basic Formulae (Field 1958)
- iii. Excitation mechanisms (Ly- α , collisions,..)
- iv. Global evolution of the spin temp.
- v. Patchy evolution
- vi. Simulation results

Key Probes of Reionization

- CMB (integral constraint)
 - Redshifted 21 cm emission (absorption)
 - 21 cm forest at high z
 - Gamma ray bursts: How many we should have to constrain reionization?
 - Luminosity function of first objects, e.g., Galaxies: Recent results from the new WFC3 aboard HST.
-
- Background detections: IR, soft x-ray.
 - Lyman- α absorption system: ionization, metallicity, thermal history, UV background, proximity effect.
 - Lyman alpha emitters
 - Metals at high redshift.
 - Using the local volume to study reionization.

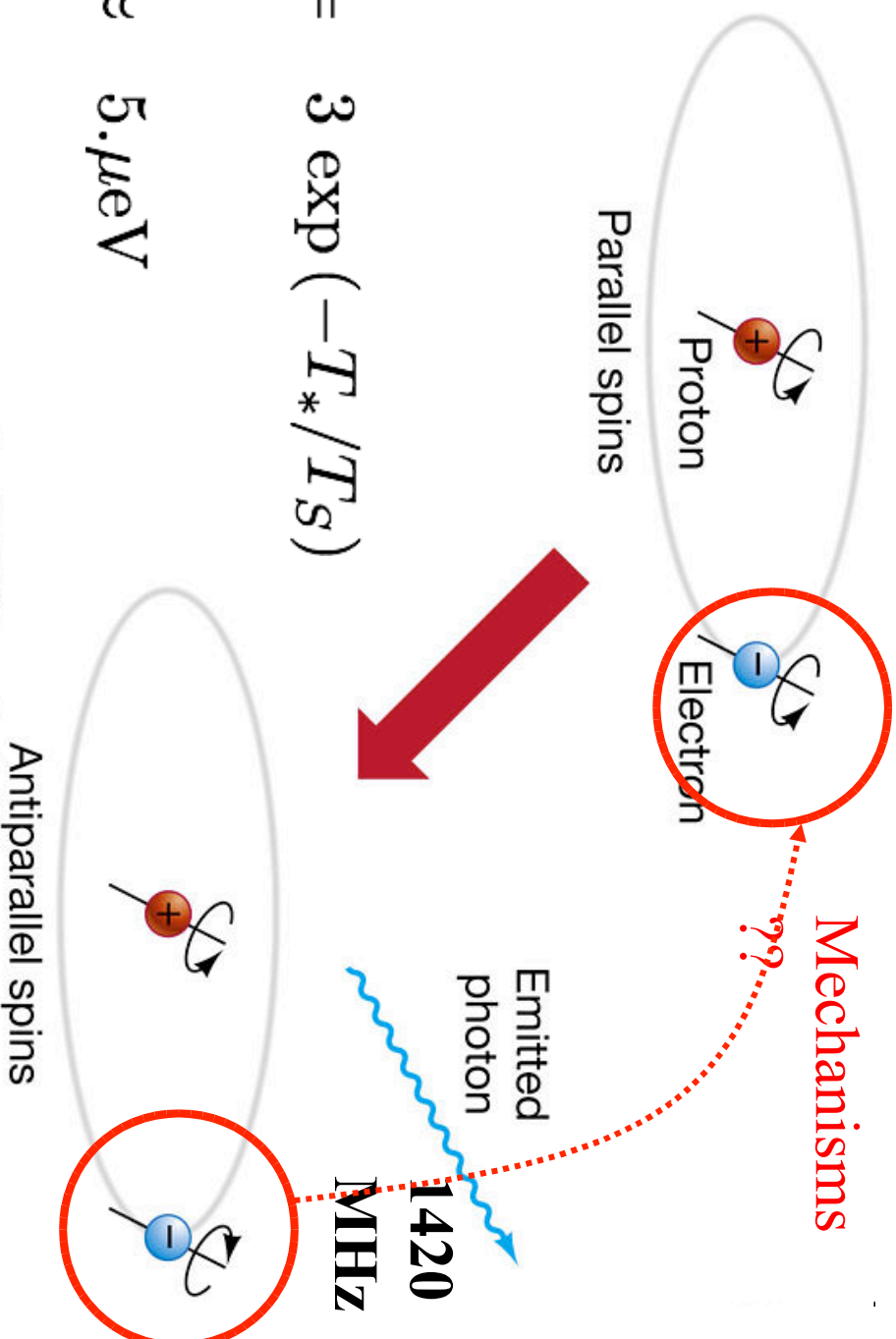
The Epoch of Reionization: Observational & Theoretical Topics

Lecture 1	Lecture 2	Lecture 3	Lecture 4
Current constraints on Reionization	Physics of the 21cm probe	EoR radio experiments	Expected Scientific outcome
<ul style="list-style-type: none">i. CMB Polarization.ii. Lyman-α forest data.iii. Opacity of ionizing photons ('Bolton et al).iv. Temperature evolution (Theuns et al, Haiman&Hui)v. Soft Xray BG (Dijkstra ..)vi. IR BG (HESS results)vii. HST WPC3 results	<ul style="list-style-type: none">i. Basic Formulae (Field 1958)ii. Excitation mechanisms (Ly-α, collisions,..)iii. Global evolution of the spin temp.iv. Patchy evolutionv. Simulation results	<ul style="list-style-type: none">i. Current & future experiments.ii. Key parameters in experiments.iii. Observational issues: uv coverage, foregrounds, ionosphere, instrument, noise.iv. Extraction issues.v. Calibration.vi. Polarization.	<ul style="list-style-type: none">i. Cosmology: Density field, ionization frac. Redshift distort, power spect.ii. First sourcesiii. Ionization historyiv. Dark ages and history of spin temperature.v. The future.

Historic overview

- H.C. van de Hulst (inspired by J. Oort) showed the potential of the 21 cm transition in astronomy – 1945
- The first astronomical observation of the 21 cm: H.I. Ewen & E.M. Purcell (1951, Nat. 168, 356)
- C.A. Muller & J.H. Oort (1951, Nat. 168, 357-8)
- Excitation mechanism Wouthuysen (1952). Field (1958, 1959) gave the proper framework.
- Importance for cosmology was inspired by Zel'dovich's top down scenario.
- Scott & Rees (1992) pointed out that a signal could be detected from high z 21 cm.
- Madau, Meiksin & Rees (1997) were the first to consider the interplay between the first sources and the 21 cm transition.
- Over the years many observational attempts failed. Shaver et al. 1999 argued that we can observe high redshift 21 cm radiation.

21-cm Physics

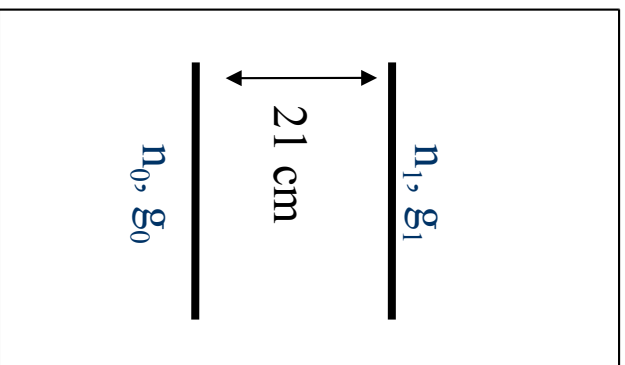


$$\frac{n_1}{n_0} = 3 \exp(-T_*/T_S)$$

$$T_* \approx 5. \mu\text{eV}$$

Lifetime of ~ 10 Myrs

The 21 cm transition



- The value of the T_s is given by:

$$T_s^{-1} = \frac{T_{CMB}^{-1} + x_c T_k^{-1} + x_\alpha T_k^{-1}}{1 + x_c + x_\alpha}$$

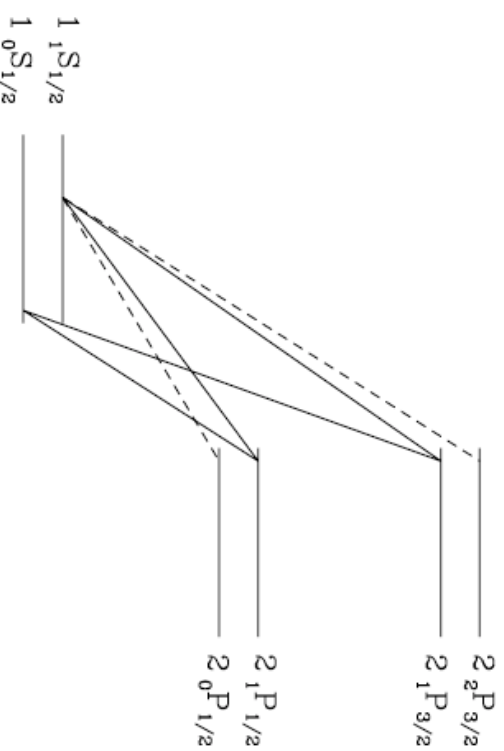
Field 1958

Madau et al 98

Ciardi&Madau 2003

Lyman- α Coupling

- The Wouthuysen-Field effect, also known as Lyman-alpha pumping.



Dominant in both in the case of stars and Black-holes, due to photo and collisional excitations, respectively.

Wouthuysen 1952

Field 1958

of the larger component. Because of the slight depth of eclipse and the trouble with comparison stars, the above results by themselves cannot be considered as anything more than suggestive. However, E. F. Carpenter's observations taken in the blue, yellow, and ultra-violet on this night and the preceding one, show this effect very clearly and leave little doubt of its reality.

It should further be noted that if the present fragmentary results prove to be a fair sample, the system is free from those erratic light changes which add such complexities to the interpretation of other systems of this sort.

*Pleasant and Cook Observatories,
University of Pennsylvania.*

Woolard, Edgar W. A comparison of Brown's Lunar Tables with the theory from which they were constructed.

For 60 dates at half-day intervals, from 1948 April 24.0 to May 24.0 UT, the longitude and latitude of the moon to two decimals of a second of arc and the parallax to three decimals were taken from Brown's tables and compared with values that had been computed to 5 decimals directly from Brown's theoretical expressions by the Selective Sequence Electronic Computer of International Business Machines Corporation.

Significant differences between the SSEC and the tabular values were evident in the longitude and in the latitude. The discrepancy in the longitude is very small but is systematic, the principal part apparently having a period of about a month, with an amplitude of the order of $0^{\circ}.1$; the discrepancy in the latitude is strongly periodic, with an amplitude about $0^{\circ}.15$ and a period about a month.

An analysis of these differences to determine their source appeared advisable. The SSEC computations were therefore compared in detail with the tabular computations for the longitude on 14 selected dates, and for the latitude on 12 of these dates. The differences are for the most part satisfactorily accounted for by approximations and expedients adopted by Brown and Hedrick in the construction of the tables to facilitate their practical use, and are within the standards of accuracy that were set for the tables. The large discrepancy in the latitude, however, is principally due to an oversight in the tables; in constructing the tables, the effect of the long period variations of the lunar inclination upon several of the large terms in the latitude was inadvertently included twice.

The resulting error in the tabular latitude is large enough to be detected in observations; it has been found in a comparison of the tabular latitude with the observed latitude obtained with the 6-inch transit circle at the U. S. Naval Observatory during 1929-1949.

*U. S. Naval Observatory,
Washington, D. C.*

Wouthuysen, S. A. On the excitation mechanism of the 21-cm (radio-frequency) interstellar hydrogen emission line.

The mechanism proposed here is a radiative one: as a consequence of absorption and re-emission of Lyman- α resonance radiation, a redistribution over the two hyperfine-structure components of the ground level will take place. Under the assumption—here certainly permitted—that induced emissions can be neglected, it can easily be shown that the relative distribution of the two levels in question, under stationary conditions, will depend solely on the shape of the radiation spectrum in the $L\alpha$ region, and not on the absolute intensity.

The shape of the spectrum of resonance radiation, quasi-imprisoned in a large gas cloud, could only be determined by a careful study of the "scattering" process (absorption and re-emission) in a cloud of definite shape and dimensions. The spectrum will turn out to depend upon the localization in the cloud.

Some features can be inferred from more general considerations. Take a gas in a large container, with perfectly reflecting walls. Let the gas be in equilibrium at temperature T_1 , together with Planck radiation of that same temperature. The scattering processes will not affect the radiation spectrum. One can infer from this fact that the photons, after an infinite number of scattering processes on gas atoms with kinetic temperature T_1 , will obtain a statistical distribution over the spectrum proportional to the Planck-radiation spectrum of temperature T_1 . After a finite but large number of scattering processes the Planck shape will be produced in a region around the initial frequency.

Photons reaching a point far inside an interstellar gas cloud, with a frequency near the $L\alpha$ resonance frequency, will have suffered on the average a tremendous number of collisions. Hence in that region, which is wider than the optical depth of the cloud is for the Lyman radiation, the Planck spectrum corresponding to the gas-kinetic temperature will be established

as far as the shape is concerned. Because, however, the relative occupation of the two hyperfine-structure components of the ground state depends only upon the shape of the spectrum near the $L\alpha$ frequency, this occupation will be the one corresponding to equilibrium at the gas temperature.

The conclusion is that the resonance radiation provides a long-range interaction between gas atoms, which forces the internal (spin-)degree of freedom into thermal equilibrium with the thermal motion of the atoms.

*Institute for Theoretical
Physics of the City University,*

Zechiel, Leon N. and Geoffrey Keller. A survey of eclipsing binary systems showing apsidal motion.

Thirty eclipsing binary systems of known or suspected apsidal motion were analyzed to determine whether a correlation could be made between the mass distribution within the stars and the spectral type. A set of combined photometric and spectroscopic elements for each system was assembled. Some systems have not been observed spectroscopically, and the values of the eccentricity and the apsidal period had to be estimated from photometric data alone in these cases. The data has been tabulated for all systems which have been adequately observed. Fourteen cases in which apsidal motion has been indicated, but for which the data are insufficient to support detailed analysis, were rejected.

The final sets of elements for each system were analyzed by the method of Sterne, yielding the apsidal coefficients, k_2 , which are a measure of the degree of central condensation of the mass of the stars. Values of the effective polytropic index of each star were obtained from the quantities k_2 in the usual manner. The absolute dimensions of the systems were derived from the elements by various methods suited to the data available in each case.

The final results were embodied in a table, and a plot of the effective polytropic index versus the spectral type was made. A similar plot was constructed from the analysis by Russell in 1930. A comparison shows considerable change in the plot due to the reclassification of the spectra of several of the stars and to the inclusion of new

data. There appears to be a limitation of k_2 to values between 2.9 and 4.1, with the lower values tending to be associated with earlier spectral types. The ratio of central density to mean density is 54 for a polytrope of index 3.0 and 614 for a polytrope of index 4.0. While the stars in this survey were not assumed to be polytropes these two cases represent models having values of k_2 corresponding roughly to the observed range. The spectral types represented in the survey ranged from O8.5 to F2.

*Perkins Observatory,
Delaware, Ohio.*

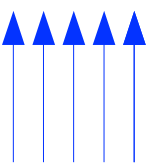
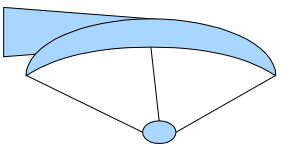
TITLES OF ADDITIONAL PAPERS PRESENTED AT THE MEETING IN CLEVELAND, OHIO

- Anderson, J. Pamela. The position of the moon at the time of the 1948 eclipse.
- Bidelman, W. P. and W. W. Morgan. A remarkable O-type star.
- Binnendijk, L. The space distribution of interstellar material in the Milky Way.
- Boh, Bart J. and Margaret Olmsted. Magnitude standards for the southern hemisphere.
- Cook, Allan F. II. Radiative equilibrium in a hydrogen atmosphere.
- Eckert, Rebecca B. Jones and H. K. Clark. A precise method of measuring the solar constant.
- Gemart, Sel H. Note on a graphical method for the prediction of occultations.
- Gouldberg, Leo, R. R. McMahon, O. C. Mohler and A. K. Pierce. Identification of CO in the solar atmosphere.
- Harwood, Margaret. The nova-like variable CM Aquilae.
- Hemmlsen, S. W. Note on the kinematics of the moon's motion.
- Johnson, Harold L. Magnitude systems.
- Mickellar, Andrew, G. J. Oggers and L. H. Aller. The Chromospheric K-line during the recent eclipse of 31 May 1948.
- Morgan, D. D. Field techniques for occultation observations.
- Mills, John. The genesis of Saturn and its rings.
- Neuman, J. and C. D. Shane. A model of spatial distribution of galaxies. Preliminary report.
- O'Keefe, John A. and J. Pamela Anderson. Calculation of the earth's radius from occultation data.
- Osterbrock, Donald A. The time of relaxation for stars in a fluctuating density field.
- Painy, T. N. and John A. O'Keefe. Progress on the measurements of darkening at the sun's limb from the results of the 1948 eclipse.
- Scoville, R. M. Theoretical counterparts of certain observable distributions relating to galaxies.
- Swope, Henrietta H. Photographic magnitudes and colors in the globular cluster NGC 6597.
- Thomson, Warren J. The path and orbit of the detonating meteor of August 29, 1951.
- White, Marvin S. Note on the accuracy of Hayn's charts as measured by photoelectric observation.
- Wriebel, Marshall H. On the decay of a primeval stellar magnetic field.
- Wyke, C. C. The path and orbit of the detonating meteor of July 28, 1951.

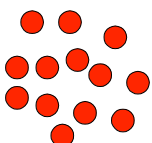
Collisional Coupling

- H-H collisions that excite the 21 cm transition. This interaction proceeds through electron exchange.
- H-e collisions. Especially important around primordial X-ray sources (mini-quasars).
 - This effect might also excite Lyman-alpha transition which adds to the $T_s - T_{\text{CMB}}$ decoupling efficiency.

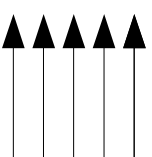
δT_b , The Brightness Temperature



T_b



T_s



T_γ

$$T_b(\nu) = T_s (1 - e^{-\tau_\nu}) + T_\gamma(\nu)e^{-\tau_\nu}$$

$$\delta T_b(\nu) \equiv T_b - T_\gamma = (T_s - T_\gamma) (1 - e^{-\tau_\nu})$$

Where the optical depth is given by:

$$\tau_\nu = \int ds \sigma_{01} (1 - e^{-E_{10}/k_B T_s}) \phi(\nu) n_0$$

$$\tau_\nu \approx \sigma_{01} \left(\frac{h\nu}{k_B T_s} \right) \left(\frac{N_{HI}}{4} \right) \phi(\nu)$$

$$\sigma_{01} \equiv \frac{3c^2 A_{10}}{8\pi\nu^2}$$

$A_{10} = 2.85 \times 10^{-15} \text{ s}^{-1}$ is the spontaneous emission coefficient.

N_{HI} is the column density of HI; 4 accounts for fraction in singlet state $\phi(\nu)$ is the line profile.

An accurate calculation of the optical depth at a given redshift, which takes into account line profile broadening due to Hubble expansion and casts the relation in terms of number density, yields:

$$\begin{aligned} \tau_{\nu_0} &= \frac{3}{32\pi} \frac{hc^3 A_{10}}{k_B T_S \nu_0^2} \frac{X_{HI} n_H}{(1+z) (dv_{\parallel}/dr_{\parallel})} \\ &\approx 0.0092 (1+\delta) (1+z)^{3/2} \frac{X_{HI}}{T_S} \left[\frac{H(z)/(1+z)}{dv_{\parallel}/dr_{\parallel}} \right] \end{aligned}$$

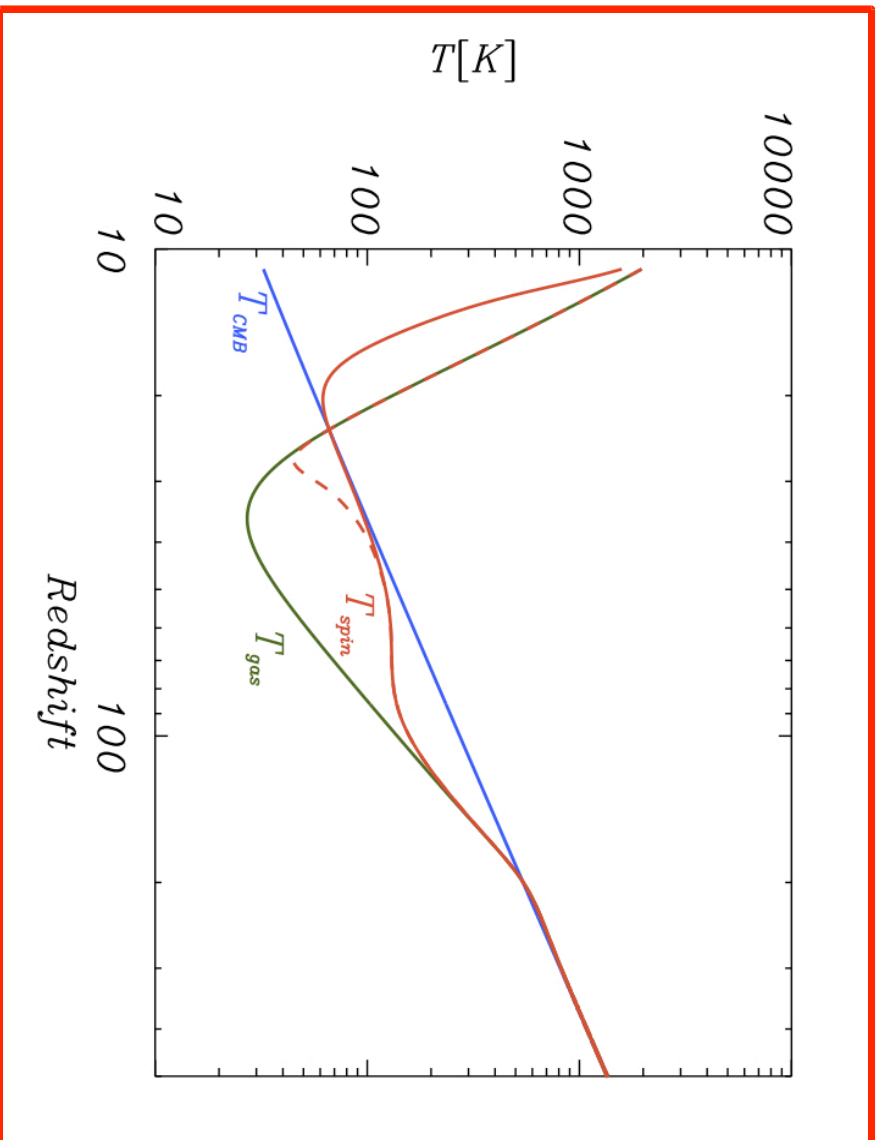
δT_b : Brightness temperature

$$\delta T_b \approx 28 \text{mK} (1 + \delta) x_{\text{HI}} \frac{T_s - T_{\text{CMB}}}{T_s} \frac{\Omega_b h^2}{0.02} \left[\frac{0.24}{\Omega_m} \left(\frac{1+z}{10} \right) \right]^{\frac{1}{2}}$$

The diagram illustrates the components of the brightness temperature equation. The equation is shown as a product of three main terms, each enclosed in a box. The first term, $(1 + \delta)$, is enclosed in a red box. The second term, $x_{\text{HI}} \frac{T_s - T_{\text{CMB}}}{T_s}$, is enclosed in a blue box and is further divided into two sub-components: 'Astrophysics' and 'Cosmology'. The third term, $\frac{\Omega_b h^2}{0.02} \left[\frac{0.24}{\Omega_m} \left(\frac{1+z}{10} \right) \right]^{\frac{1}{2}}$, is enclosed in a red box. The entire equation is labeled as $\delta T_b \approx 28 \text{mK}$ on the left.

- The Interpretation might be very complicated
- Notice that the signal in absorption can be much smaller

The Global evolution of the Spin Temperature



At $z \sim 20$ T_s is tightly coupled to T_{CMB} . In order to observe the 21 cm radiation decoupling must occur.

Heating much above the CMB temp. and decoupling do not necessarily occur together.

Loeb & Zaldarriaga 2004, Pritchard & Loeb 2008,
Baek et al. 2010, Thomas & Zaroubi 2010

$$T_{CMB} \propto 1 + z$$

$$T_k \propto (1 + z)^2$$

$$\begin{aligned} \text{Compton heating rate} \quad \epsilon_{comp} &\approx \frac{n_e k_B (T_{CMB} - T_k)}{t_{comp}} \end{aligned}$$

$$\begin{aligned} \text{Compton cooling time} \quad t_{comp} &= \frac{3m_e c}{8\sigma_T u_\gamma} \\ u_\gamma &\propto T_{CMB}^4 \end{aligned}$$

This drives the Compton heating rate to almost zero

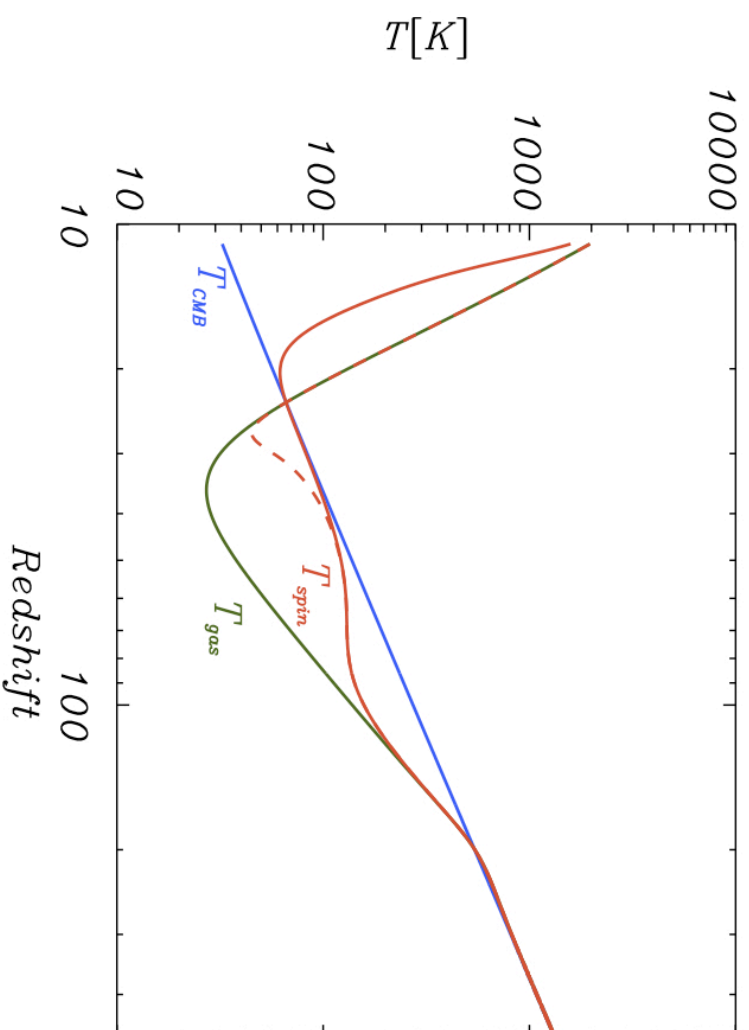
The redshift of thermal decoupling is about 200

(proper calculation could be done with the publicly available code RECFAST)

The Spin Temperature Prior to the EoR



Only feasible from
the Moon



Ionization sources

Mean free path

$$\langle l_E \rangle \approx \frac{1}{n_H \sigma_H(E)}$$

Bound-free
Cross section

$$\sigma_H(E) = \sigma_0 (E_0/E)^3$$

$$n_H = 2.2 \times 10^{-7} \text{ cm}^{-3} (1+z)^3$$

$$\sigma_0 = 6 \times 10^{-18} \text{ cm}^2$$

$$E_0 = 13.6 \text{ eV}$$

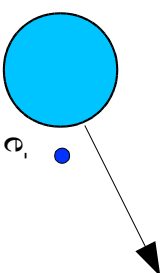
At $z = 9$: For $E = E_0$

$\langle l_E \rangle \approx 2 \text{ kpc comoving}$

For $E = 1 \text{ keV}$

$\langle l_E \rangle \approx 1 \text{ Gpc comoving}$

UV photons

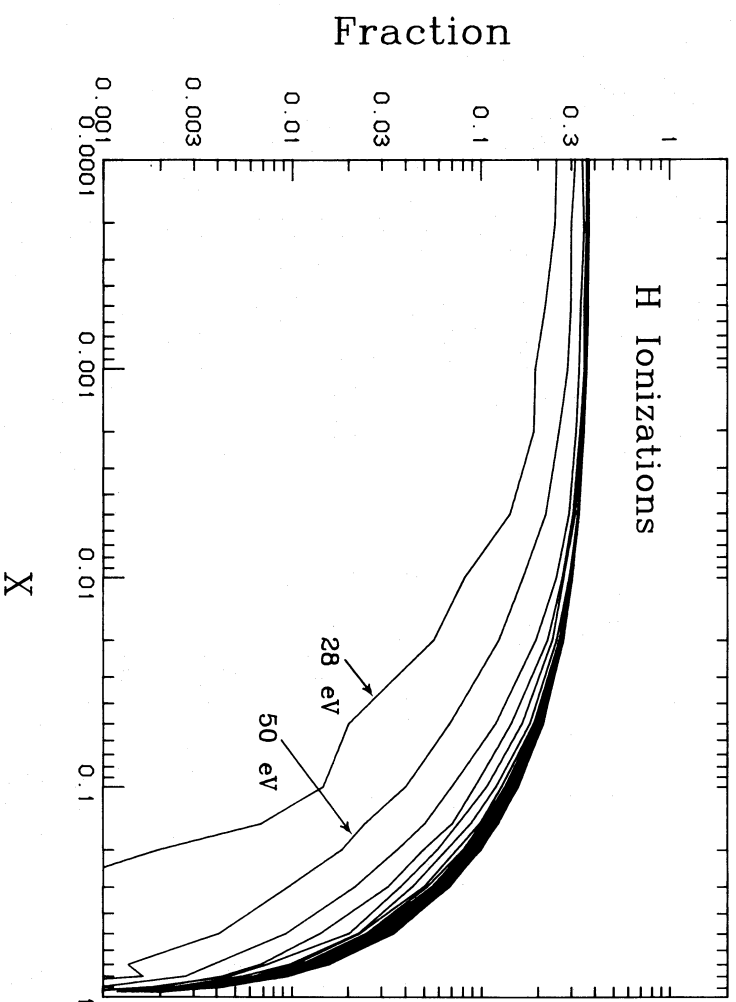


Large cross section but ejected electron has low energy

X-ray photons

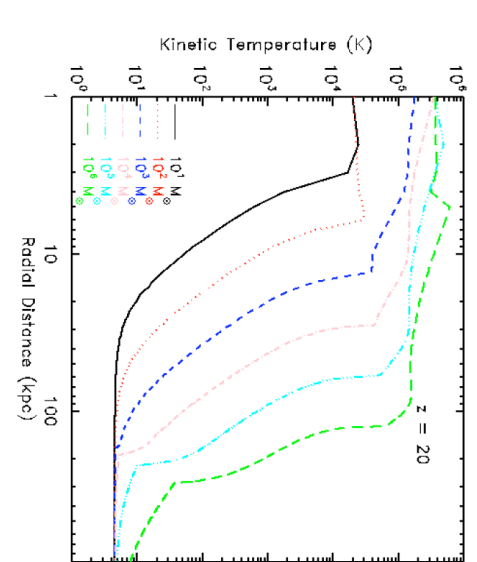
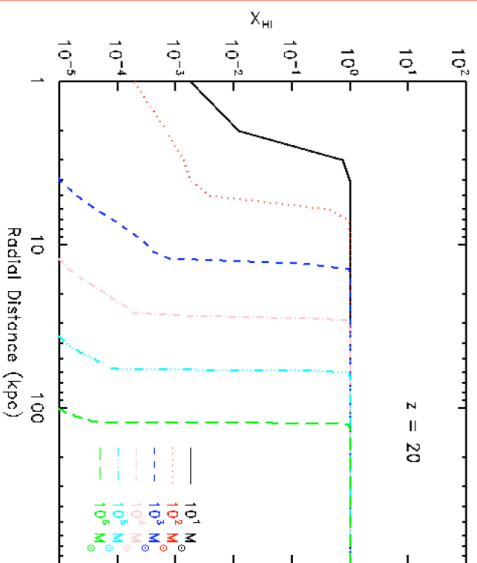
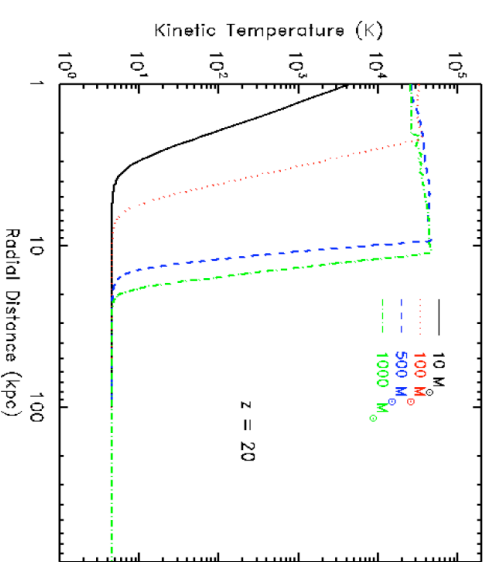
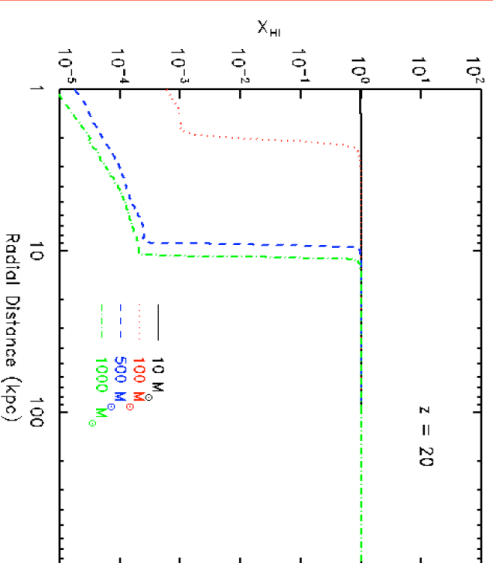


Low cross section but ejected electron has high energy



The fraction of photon energy that goes to reionization, heating and excitation is roughly 1:1:1 as calculated with Monte-Carlo radiative transfer code by Shull & van Steenberg (1986) and Valdes et al. 2009.

The signal: Stars vs. Miniqsos

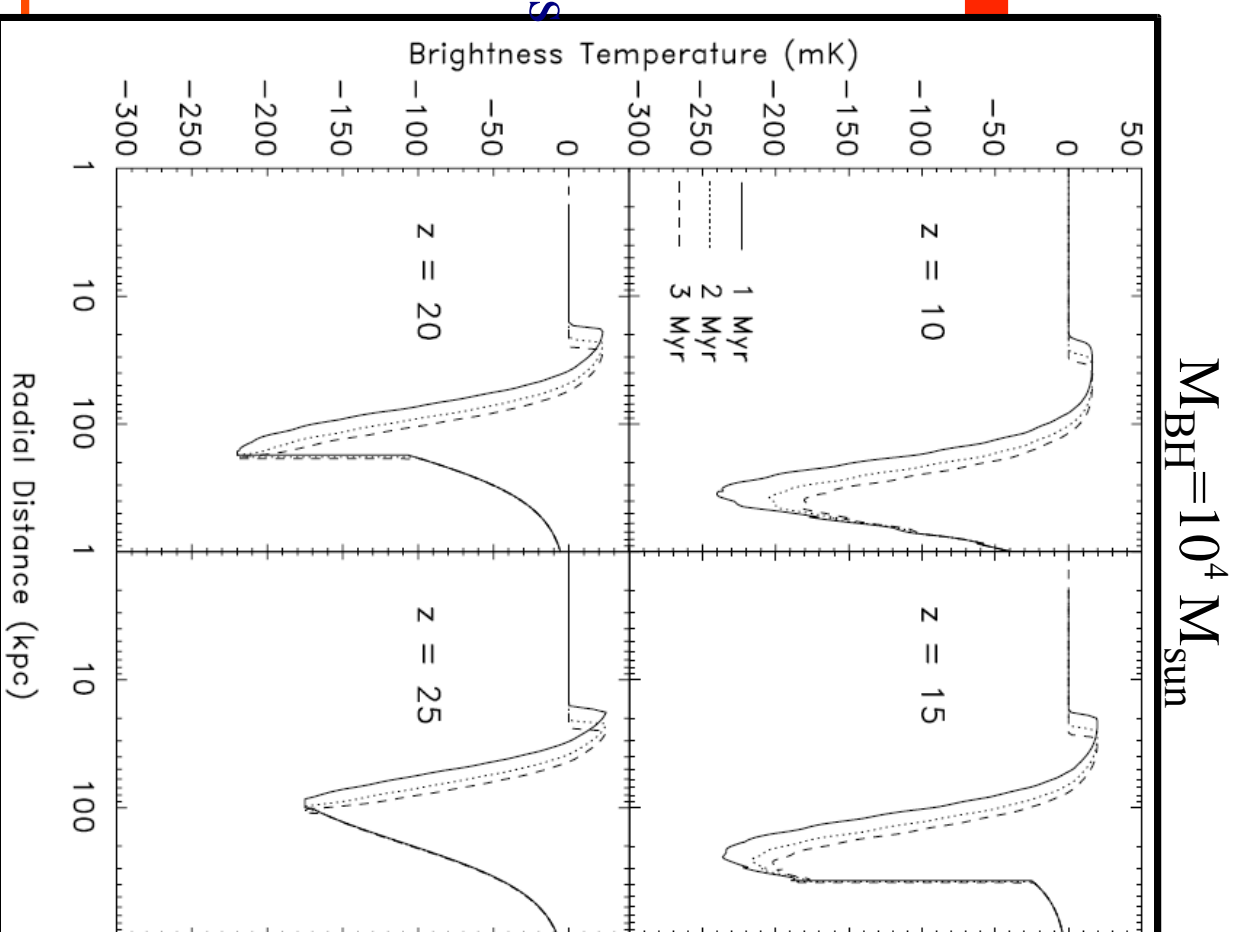


Thomas &
Zaroubi 2008

What happens around a high
Redshift x-ray source

Kinetic temperature is greatly
heated just beyond the HII region,
but further out it has been
adiabatically cooled.

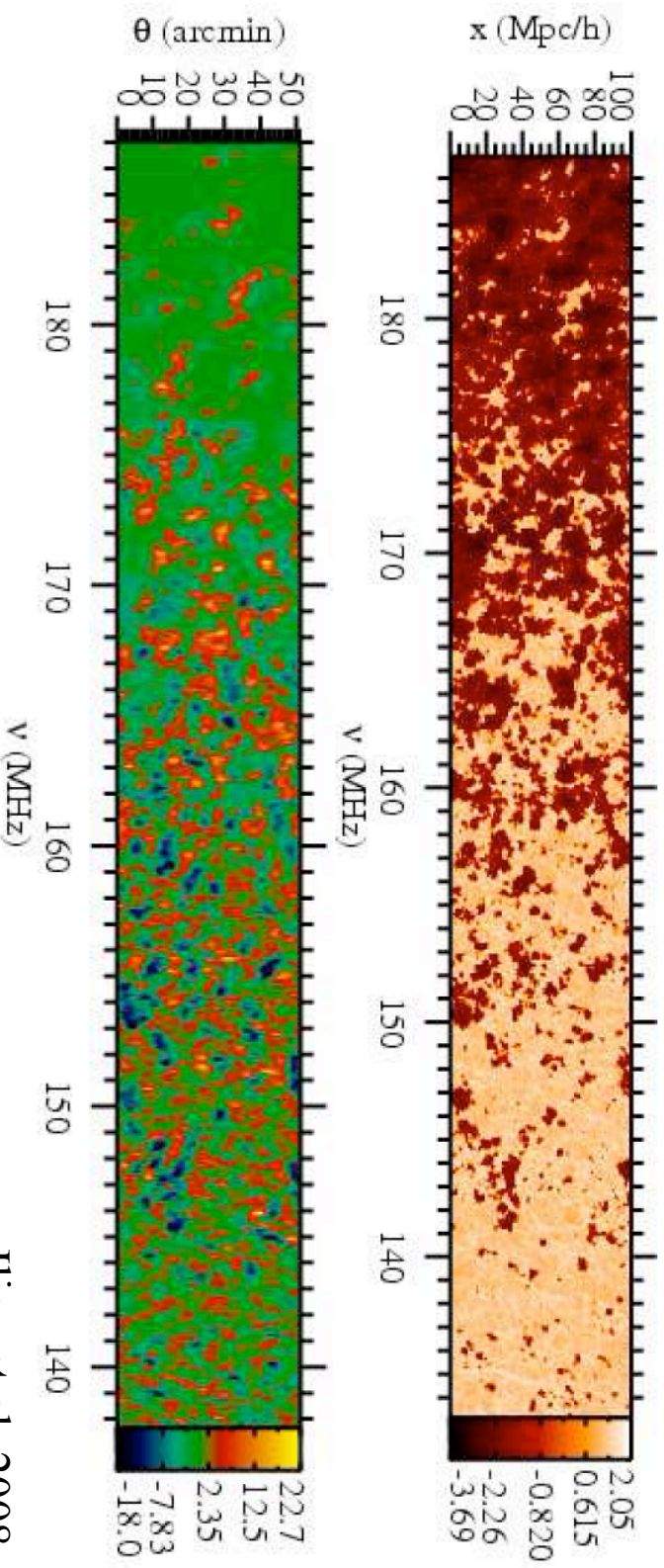
21 cm absorption strongly dominates
over the inner emission core



Simulations of the EoR

- Cosmological Hydro simulations:
 - 1- High enough resolution to resolve halos in which ionization sources form.
 - 2- Span Large Scales as well as small scales, especially since designed arrays have small l' res.
 - 3- In certain cases DM only simulations are sufficient.
- Out of equilibrium Radiative Transfer:
 - 1- Source and their flux.
 - 2- Ionization of H and He (not always done).
 - 3- Heating due to the radiative processes.
 - 4- Spin temp decoupling ($\text{Ly}\alpha$ RT).
- It is very difficult to account for all the physical aspects of the problem and approximations are normally made.

Results from 3D RT

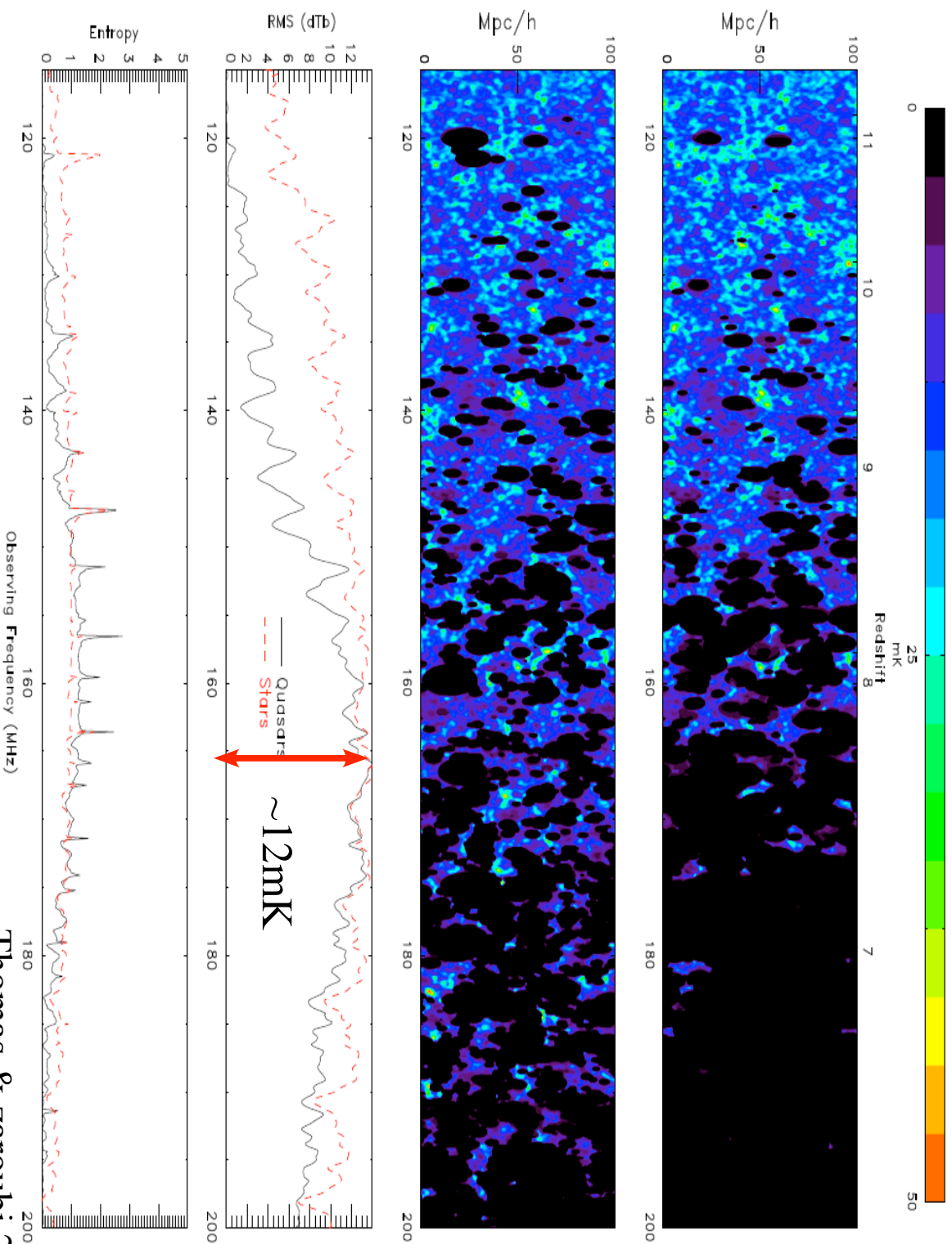


Iliev et al. 2008

At half ionization the signal rms is about 8mK

~~$$\delta T_b \approx 28 \text{mK} (1 + \delta) x_{HI} \frac{T_s - T_{CMB}}{T_s} \frac{\Omega_b h^2}{0.02} \left[\frac{0.24}{\Omega_m} \left(\frac{1+z}{10} \right) \right]^{\frac{1}{2}}$$~~

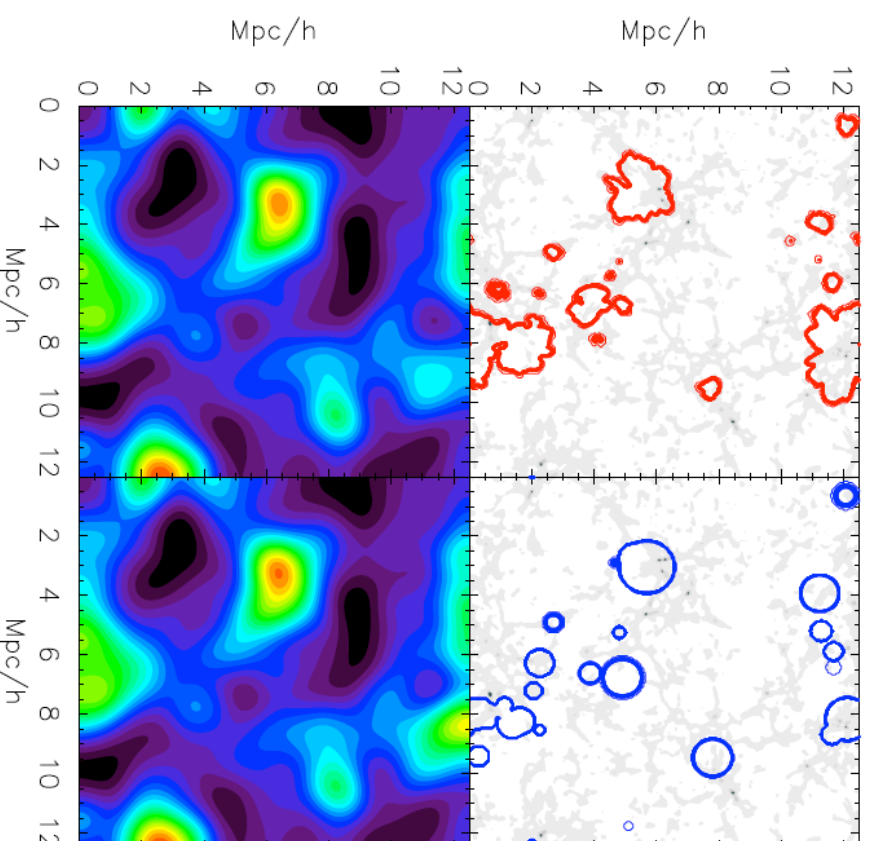
Results from approximate methods



Thomas & zaroubi 2008

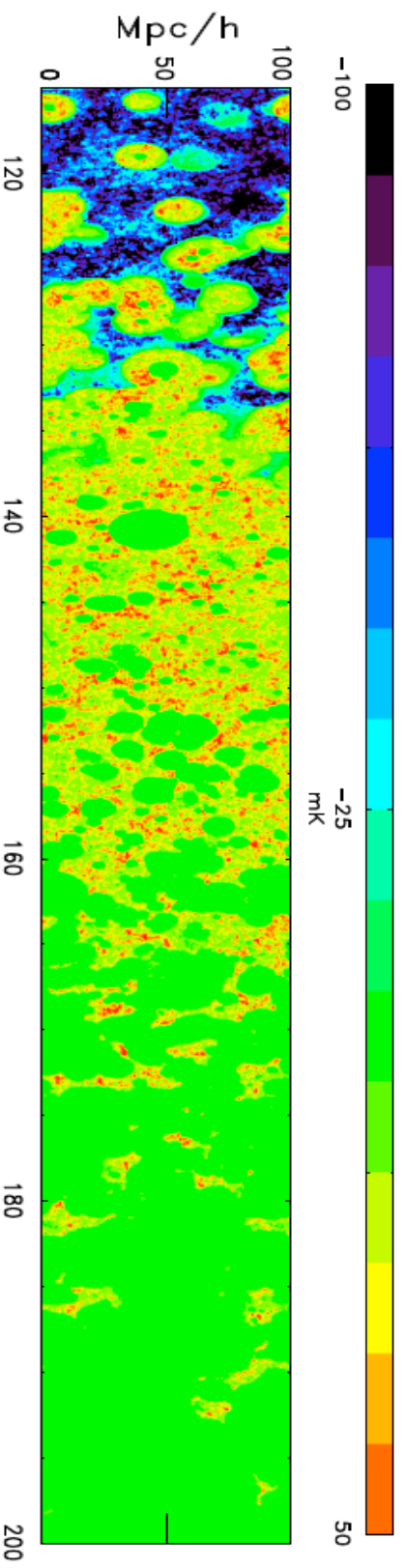
Full vs. approximate simulations

- Full 3D RT simulations are more accurate but computationally expensive. They provide crucial insight about the physical processes (especially on small scales).
- Approximate methods are less accurate but easier to produce and allow for an exploration of the parameters space. This is especially important for interpretation of the data



Spin Temperature issues

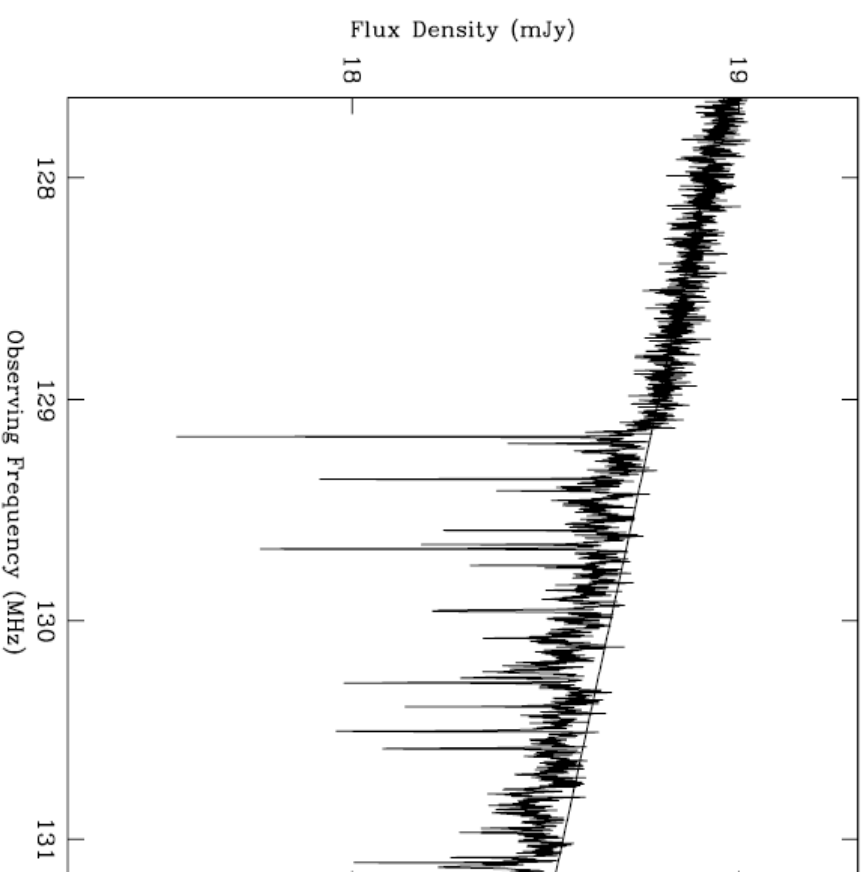
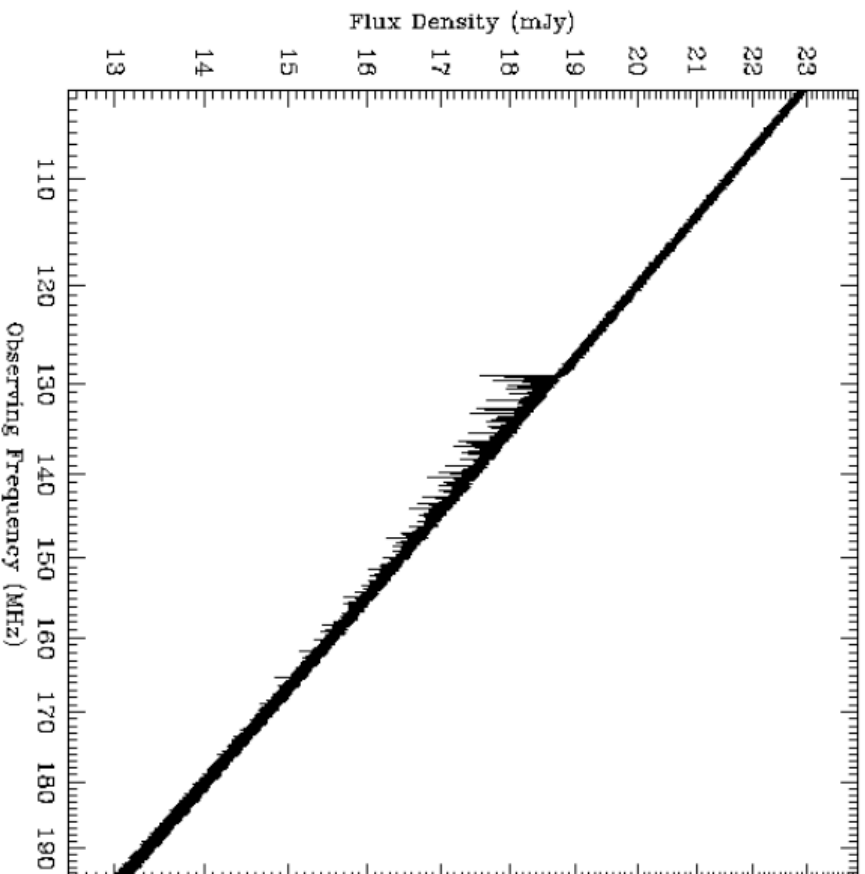
In case the spin temp. is of the order the CMB temp. or smaller an absorption signature is expected at high redshifts.



$$\delta T_b \approx 28 \text{mK} (1 + \delta)^{x_{HI}} \frac{T_s - T_{\text{CMB}}}{T_s} \frac{\Omega_b h^2}{0.02} \left[\frac{0.24}{\Omega_m} \left(\frac{1+z}{10} \right) \right]^{\frac{1}{2}}$$

Thomas & Zaroubi 2010
See also Baek et al. 2010

The 21 cm forest



Simulated spectrum from 100 MHz to 200 MHz of a source with $S_{120} = 20$ mJy at $z=10$ using the Cygnus A spectral model and SKA noise

Summary

- 21 cm line is a very promising probe of the EoR and the Dark Ages.
 - It tracks the evolution of reionization and the thermal history of the IGM in time and space.
 - The signal is of the order of $10 \mu\text{K}$ in emission and $100 \mu\text{K}$ in absorption.
-